Future Circular Collider

PUBLICATION

Magnetic refrigeration down to 1.6 K for the future circular collider e^+e^-

Tkaczuk, Jakub (CEA (FR)) *et al.*

29 August 2017

The research leading to this document is part of the Future Circular Collider Study

Magnetic refrigeration down to 1.6 K for the future circular collider e^+e^-

Jakub Tkaczuk,* François Millet,† Jean-Marc Duval, and Bernard Rousset
Univ. Grenoble Alpes, INAC-SBT, F-38000 Grenoble, France
CEA, INAC-SBT, F-38000 Grenoble, France
(Received 14 July 2016; published 11 April 2017)

High-field superconducting rf cavities of the future circular collider e^+e^- may require a kW-range superfluid helium refrigeration down to 1.6 K. Magnetic refrigeration operating below 4.2 K can be an alternative to the compression/expansion helium refrigeration. A significant difference between this application and previous magnetic refrigerator studies is its large cooling power, up to 10^3 times larger than the other designs. Principles of magnetic refrigeration are described and various technical solutions are compared. A numerical model for the static magnetic refrigerator is presented, validated, and adapted to the needs of the positron-electron version of the future circular collider. A preliminary design of magnetic refrigerator suitable for low temperature, kW-range cooling is studied.

DOI: 10.1103/PhysRevAccelBeams.20.041001

I. INTRODUCTION

High field superconducting rf cavities of the future circular collider e^+e^- (FCC) may require a kW-range superfluid helium refrigeration down to 1.6 K. Indeed, to cool down superconducting rf (SRF) cavities, helium cooling is classically used in normal state (4.5 K) or in superfluid state ($T < 2.1$ K). The SRF cavities operating temperature is selected to minimize the cost and the energy consumption of the whole accelerator infrastructure [1] including SRF cavities and cryogenic cooling as shown in Fig. 1.

If one would like to operate at optimal temperature—1.6 K (the refrigeration cost minimum in Fig. 1) the compression/expansion cycle with several cryogenic centrifugal compressors pumping in series is the current design for kW-range superfluid helium refrigeration. However, this solution presents some obvious disadvantages such as complex control of the cold compression train and long downtime after stops. It might be possible to replace the cold compressors by magnetic refrigeration or to add one magnetic refrigeration stage to an already existing system to reduce the number of cold compressors in series. Magnetic refrigerator operating below 4.2 K could be therefore an alternative to the compression/expansion helium refrigeration. A preliminary design of magnetic refrigerator suitable for low temperature, kW-range cooling is detailed in the following work.

*jakub.tkaczuk@gmail.com
†francois.millet@cea.fr

II. MAGNETIC REFRIGERATION THEORETICAL PRINCIPLES

Magnetic refrigeration is a cooling method based on the magneto-caloric effect: a reversible variation of internal energy in suitable material when external magnetic field is modified. The magnetic refrigerator working principle depends on the technical solution, the one studied below follows a Carnot-like cycle. If the magnetic field increases, depending on whether the transformation is adiabatic or isothermal, either the material temperature increases (phase 1 in Fig. 2) or the magnetic moments align (phase 2 in Fig. 2) [2].

The magneto-caloric material and the type of thermodynamical cycle with a practical design should be carefully chosen depending on the specific application. A relevant magneto-caloric material has to be selected for the designed temperature range (4.5 K – 1.6 K). Material commonly

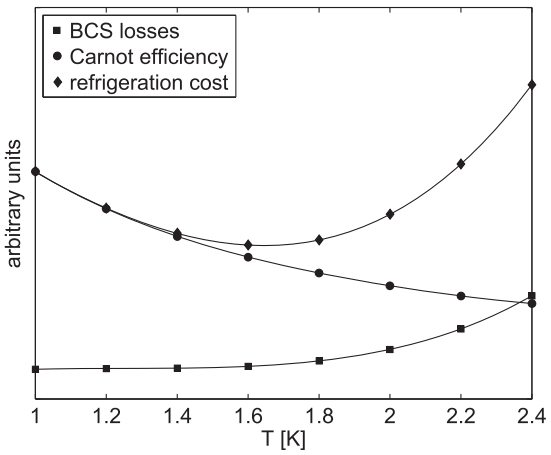

FIG. 1. Optimal operating temperature for superconducting rf cavities [1].

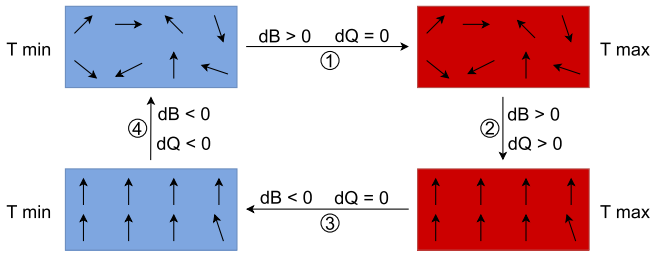

FIG. 2. Adiabatic demagnetization refrigerator cycle.

used for refrigeration down to 1 K is gadolinium gallium garnet, $Gd_3Ga_5O_{12}$ or GGG [3].

While choosing the technical implementation for the FCC application, the following objectives need to be considered: large cooling capacity, high reliability, high efficiency, and compact construction. The factors allowing comparing various designs in terms of efficiency and size (material cost) are cycle efficiency η_c [W/W] and volumetric cooling capacity [W/dm^3]—cooling capacity $\dot{Q}$ referred to the volume of magneto-caloric material V_G, ideally both coefficients should be maximized. The largest magnetization, hence the largest entropy change is characterized by the highest cycle efficiency η_c value. A comparison of various designs is performed in order to select the most suitable magnetic refrigerator technical solution for the FCC.

III. TECHNICAL SOLUTIONS

Several technical solutions have been developed in the past and are analyzed in terms of scaling to large cooling capacity.

A. CEA double acting reciprocating magnetic refrigerator

In the design developed in CEA-Grenoble in the 1980s, two stationary magnets and two moving GGG single crystals were operated in reciprocating mode [4,5]. Working pressure of two heat sources (He-I on the warm side and He-II on the cold side) were similar in order to limit the leaks. Very large cycle efficiency (>50%) was obtained thanks to the direct contact between GGG and heat sources only during the 'isothermal' transformations. The need of moving magneto-caloric material brings into question the refrigerator reliability. Increasing magneto-caloric material mass might lead to additional problems with leaks and inertia.

B. Hitachi rotary magnetic refrigerator

The rotary magnetic refrigerator was using 12 GGG pieces installed in a rotor. Thanks to this design the cooling production was almost continuous and reasonable performances were obtained ($\eta_c > 30\%$) [6]. In comparison to the reciprocating magnetic refrigerator inertia was not a critical issue but leak-tightness remained essential in the operation phase. The use of stationary magnets and the construction itself put limitations on magnetic field profile—in none of the positions zero field could have been obtained.

C. Hitachi static magnetic refrigerator

Another magnetic refrigerator constructed by Hitachi was based on static GGG and pulsed superconducting magnet [7,8]. The design took advantages of efficient heat transfer during the phase transition in "isothermal" transformations. It was assumed that stratified helium inside the heat sources can work as a static heat switch between GGG and the helium bath. While no moving parts brought the benefits of high reliability, high heat losses to the warm source were identified at the same time. They significantly reduced the cooling capacity and cycle efficiency (<15%).

D. CERN magnetic refrigerator

At CERN a magnetic refrigerator with superconducting pulsed magnets, static GGG and circulating ^{4}He was constructed [9]. It was designed to reach a cooling power of more than 10 W at 1.8 K. Due to large losses caused by constant presence of liquid helium inside the GGG (large dead volume), the refrigerator was limited in performance. The research activity was stopped before global performance measurements, after identifying the main limitations: negative influence of helium dead volume inside the GGG on cooling capacity and superfluid transition of helium present inside the magneto-caloric material occurring in every cycle.

E. MIT tandem active magnetic regenerative refrigerator

The magnetic refrigerator designed in MIT worked in tandem mode (two GGG cores operating in counterphase) with pulsed superconducting magnets and ^{3}He circulation [10]. Helium gas, in comparison to liquid, has minor influence on dead volume because of significantly lower mass. Unlike ^{4}He, ^{3}He has no superfluid transition during the whole cycle. However, using gaseous ^{3}He imposes low working pressure (50 mbar for operating at 1.8 K) and results in unsatisfying heat exchange conditions for reasonable pressure drop. Experiments showed significantly lower cooling capacity and cycle efficiency (<15%) in comparison with the calculated values.

F. Studied solution

The main parameters and a summary of described design performances are presented in Table I. A design with high volumetric cooling capacity and high cycle efficiency should be developed for FCC_ee. However, a solution which is reliable and easily scalable has to be selected. Therefore, the Hitachi static magnetic refrigerator is studied

TABLE I. Comparison of various technical solutions.

	A. CEA	B. Hitachi rotative	C. Hitachi static	D. CERN	E. MIT
Cold source temperature [K]	1.8	1.8	1.8	1.8	1.8
Warm source temperature [K]	4.2	4.2	4.2	4.5	4.2
External field variation [T]	0–4	0.5–3	0–3	0–3.5	0–2.8
Frequency [Hz]	0.8	0.5	0.4	0.2–1	0.1
Cooling capacity [W]	1.35	1.8	0.5	10[a]	0.012
$\dot{Q}/V_G$[W/dm^3]	**75.6**	**12.2**	**5.0**	-[a]	**0.7**
Cycle efficiency η_c [W/W]	**0.53**	**0.34**	**0.13**	-[a]	**0.12**

[a]Results not published.

in detail with objectives to improve its efficiency and volumetric cooling capacity.

As mentioned before, GGG is a magneto-caloric material commonly used for refrigeration in 5 K − 1 K temperature range. Its entropy can be reasonably well described using the free ion model [11]. It was compared with experimental values [12,13] and is presented in Fig. 3.

Other important GGG properties used in the following calculations are thermal conductivity, magnetization, and specific heat [13–16].

Properties of normal helium are available within HePak [17] with extended conductivity values [18].

IV. DESCRIPTION OF THE MAIN PHYSICAL PHENOMENA EXPECTED IN THE STUDIED DESIGN

The static magnetic refrigerator is schematically represented in Fig. 4. The magneto-caloric material is placed inside the cold bore of a superconducting coil with one He-I bath on its top (warm source) and one He-II bath at its bottom (cold source). During isothermal magnetization (phase 2 in fig. 2) heat is transferred from GGG to the warm source throughout boiling. During isothermal demagnetization (phase 4 in Fig. 2) heat is transferred from the cold source to GGG throughout condensation.

When the GGG temperature is larger than the cold source temperature (phases 1, 2, 3 in Fig. 2), insulation of the He-II bath is provided thanks to stratification in gaseous helium. As the gas conductivity is small (around 0.01 W/mK), the losses to the cold source have little impact on general performance.

When GGG is colder than the warm source, the stratification in liquid helium is supposed to limit the heat flow toward GGG. However, when GGG temperature falls below $T_\lambda = 2.17$ K, a thin layer of superfluid helium appears at the warm source—GGG interface. As superfluid helium conductivity is very large (up to 10^5 W/mK), strong heat exchange between the superfluid helium and colder GGG begins. This phenomena causes the largest loss in the system (more than 50% of the cooling capacity). The present design study aims at reducing these losses to achieve better efficiency for the static magnetic refrigerator.

A. Warm side heat exchange

GGG and liquid helium at the warm source interface abide by the rules of solid-liquid heat transfer during isothermal magnetization. Depending on the temperature difference between the fluid and the wall, heat exchange is guided by convection, nucleate boiling, transition boiling, or film boiling. The objective for this heat exchange with

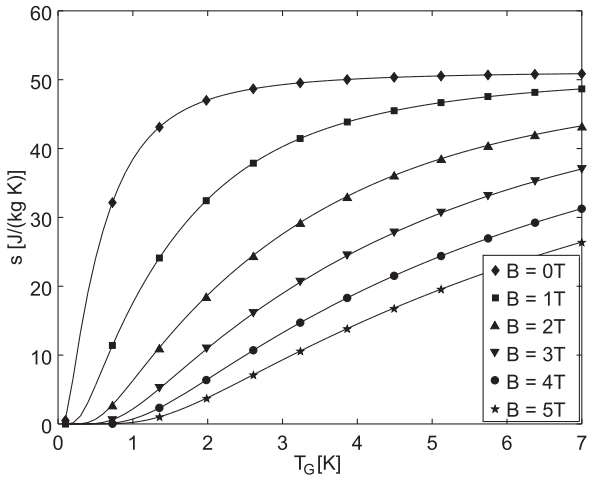

FIG. 3. GGG entropy calculated with free ion model depending on magnetic field B and temperature T.

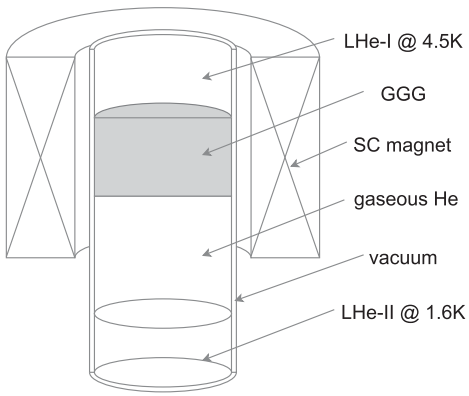

FIG. 4. Scheme of the Hitachi static magnetic refrigerator.

the warm source is to minimize the temperature difference. Good compromise between large heat flux $\dot{q}$ and limited ΔT is the nucleate boiling regime. Numerous approaches describe the heat exchange between the liquid and the solid within the nucleate boiling regime [19]. A reliable formula is the Kutateladze correlation:

$$\frac{h}{K_l}\left(\frac{\sigma}{g\rho_l}\right)^{0.5} = 3.25\times10^{-4}\left[\frac{\dot{q}c_{pl}\rho_l}{K_l\rho_v L_H}\left(\frac{\sigma}{g\rho_l}\right)^{0.5}\right]^{0.6} \times\left[g\left(\frac{\rho_l}{\mu_l}\right)^2\left(\frac{\sigma}{g\rho_l}\right)^{1.5}\right]^{0.125}\left[\frac{p}{(\sigma g\rho_l)^{0.5}}\right]^{0.7}, \tag{1}$$

where: c_p[J/kgK] is specific heat; g[m/s^2] is gravity of earth; h[W/m^{2}K] is heat transfer coefficient; K[W/mK] is thermal conductivity; L_H[J/kg] is latent heat; p[Pa] is pressure; $\dot{q}$[W/m^2] is heat flux; μ[kg/ms] is dynamic viscosity; ρ[kg/m^3] is density; σ[N/m] is surface tension. Indexes: l is liquid; v is vapor.

B. Cold side heat exchange

During isothermal demagnetization, the phase when GGG is colder than the cold source, heat is extracted from the cold source throughout condensation on the GGG surface. Heat transfer in superfluid helium for temperatures below lambda point is limited by Kapitza resistance [20]. Very large superfluid helium conductivity leads to the assumption that apart from the Kapitza layer no temperature difference is present in the condensation film.

Heat transfer by condensation is highly efficient on vertical surfaces and much less efficient on horizontal surfaces. As vertical surfaces are necessary, grooves on the GGG cold surface were introduced in Hitachi design and are taken into account in the present design study.

Heat transfer coefficient between Kapitza layer and polished GGG is depicted below [20,21]:

$$h_k = 670\cdot T_H^{3.15}\left[1+\frac{3}{2}\left(\frac{T_H-T_G}{T_H}\right)+\left(\frac{T_H-T_G}{T_H}\right)^2 +\frac{1}{4}\left(\frac{T_H-T_G}{T_H}\right)^3\right], \tag{2}$$

where T_H[K] is helium bulk temperature; T_G[K] is GGG wall temperature.

C. Internal heat losses

The following heat losses during the magnetic refrigeration cycle are considered:

1. Heat exchange between GGG and the warm source

Large temperature gradient is generated due to the contact of cold GGG with liquid helium at the warm interface. Magneto-caloric effect is lowered by diffusion from the warm source. Diffusion with cold production is defined:

$$\frac{\partial T}{\partial t} = D\left[\frac{\partial^2 T}{\partial x^2}+\frac{\rho}{K}\left(M+\frac{1}{c_B}\frac{\partial T}{\partial B}\Big|_s\right)\frac{dB}{dt}\right], \tag{3}$$

where $B[T]$ is magnetic field; $c_B = T\frac{\partial S}{\partial T}|_B$ is specific heat at constant field; D[m^2/s] is thermal diffusivity; K[W/mK] is thermal conductivity; M[Am^2/kg] is magnetization referred to mass; t[s] is time; T[K] is temperature along the x-axis; ρ[kg/m^3] is density. Due to the large conductivity in superfluid helium and presence of the Kapitza resistance at the interface, it is assumed that the fluid temperature does not fall below $T_\lambda - \epsilon$ at the warm source interface (where ϵ is the smallest significant value), when GGG temperature is lower than T_λ.

2. Heat exchange between GGG and the cold source

Stratification inside the helium gas in He-II bath ensures partial insulation of the cold source. Small heat losses appear due to the conduction inside low thermal conductivity gas.

3. Solid conduction and Rollin film losses to the cold source

Rollin film is a creeping effect present on the walls of the superfluid helium container. The distance between the He-II meniscus and the GGG should be large enough to avoid heat transfer in the Rollin film. If the conduction inside the vessel wall is larger than 800 μW/m the Rollin film losses can be neglected in comparison to solid conduction ones.

4. Radiation heat loss from vacuum enclosure to the cold source

According to Stefan-Boltzmann law, radiation is proportional to the fourth power of the surface absolute temperature and in cryogenic design with thermal shielding its value is low and is neglected in the preliminary design.

D. Magnet design and AC-losses

In addition to the thermal calculations, magnet design needs to be performed and validated. Its main goal is to provide the required field profile inside the magneto-caloric material with the lowest possible dissipation. For these types of applications at low temperatures ($T < 5$ K), available superconducting magnets are particularly well adapted because they have no Joule losses. However, with varying magnetic field, AC-losses should be limited all along the magnetic refrigeration cycle.

AC-losses appear in superconducting material, when exposed to external, pulsed magnetic field. The losses can be lowered using suitable superconducting wire and matrix

for the magnet construction. In the first approximation, the parameters which influence the AC-losses P_{AC} can be summarized as superconducting filament diameter ϕ_f, transverse resistivity of the matrix ρ_t and twist pitch of superconducting wire L_p, as detailed in the following formula [22]:

$$P_{\mathrm{AC}} = \sum_i V^i_{\mathrm{coil}} \left(\frac{8}{3\pi} \phi_f f J_c \overline{B^i} + \frac{1}{2\rho_t} L_p^2 f^2 \overline{B^{i2}} \right), \quad (4)$$

where f[Hz] is current frequency; J_c[A/m^2] is average critical current density; L_p[m] is wire twist pitch; V^i_{coil}[m^3] is coil volume in which field $B^i[T]$ can be approximated with constant value; ρ_t[Ωm] is transverse resistivity; ϕ_f[m] is superconducting filament diameter. The first term describes the hysteresis loss in the filament, and the second one describes the coupling loss in the matrix.

V. MODEL VALIDATION

A. Input parameters

Previously described phenomena were combined in a numerical model and a global simulation was performed to compare the results with previously published experimental data [7,8]. Input parameters are summarized in table II.

In the simulation the cycle calculations are iterative—GGG thermodynamic state is calculated in every time-step:

$$dS^\tau = \frac{\partial \dot{Q} d\tau}{T_G^{\tau-1}},$$

where dS^τ[J/K] is entropy change between $\tau - 1$ and τ time-steps; $\partial \dot{Q}$[W] is heat exchanged by GGG in time $d\tau$; $T_G^{\tau-1}$[K] is temperature in the previous time-step.

First, the ideal Carnot cycle is modeled with the magnetic material properties and ideal heat exchange assumption, as shown in Fig. 5. Then the heat exchange conditions in boiling and condensation phases are introduced and additional temperature differences appear. They are caused by limited heat fluxes in the processes of condensation and boiling. Finally, heat losses are superposed with these results in order to obtain the performances of a complete static magnetic refrigerator cycle.

TABLE II. Validation parameters.

Cold source temperature [K]	1.8
Warm source temperature [K]	4.2
External magnetic field [T]	0–3
GGG diameter [cm]	5
GGG length [cm]	5
GGG mass [kg]	0.7
Frequency [Hz]	0.4

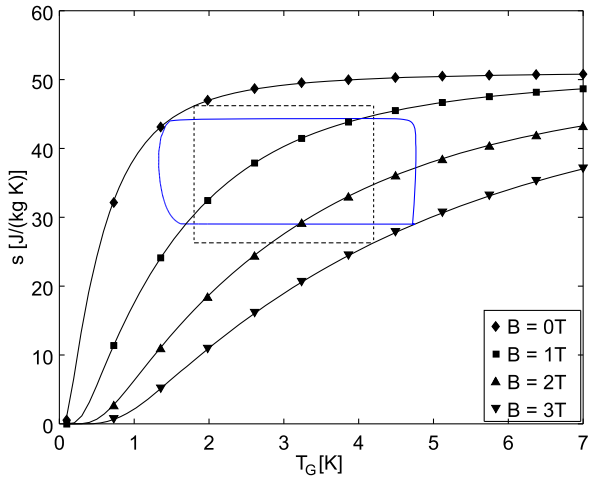

FIG. 5. Carnot cycle (dashed) and thermodynamic cycle taking into account heat exchange conditions on warm and cold sides (blue) of the Hitachi static magnetic refrigerator, without heat losses.

B. Heat losses

When GGG temperature falls below T_λ strong heat exchange appears at the boundary between GGG and helium implying large thermal gradient inside the GGG. While low thermal diffusivity prevents whole GGG from warming up, these losses have strong impact on overall cooling capacity.

During heat exchange with the cold source (5.5 s – 10 s) thermal diffusivity can be treated as a quasiconstant for the heat losses calculations ($D = 3 \times 10^{-4}$ m^2/s), as presented in Fig. 6. In this transformation the loss caused by GGG-warm source heat exchange is responsible for 95% of the total, internal heat losses (for chosen GGG geometry and refrigerator design).

Heat loss caused by AC-losses is treated as an external loss, it does not affect the GGG itself but it increases the

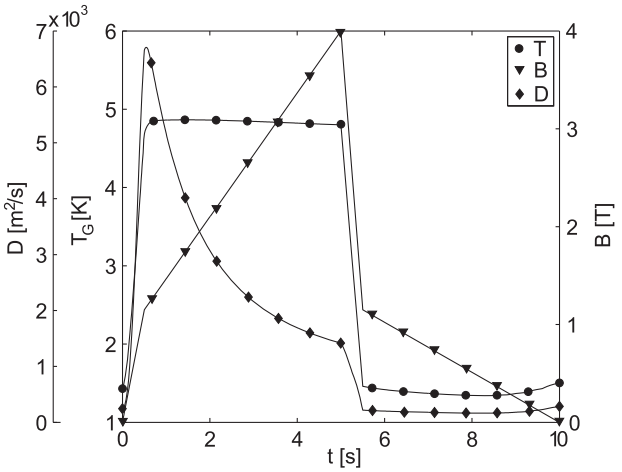

FIG. 6. Thermal diffusivity change during complete cycle.

TABLE III. Mathematical model verification.

	Model	Experimental
Internal heat losses [W]	1.0	0.95
AC-losses [W]	1.1	1.7
Cooling capacity [W]	0.55	0.5
Volumetric cooling capacity [W/dm^3]	5.0	5.0
Cycle efficiency η_c [W/W]	0.12	0.13

warm source capacity need. With data provided by Hitachi [7], additional assumptions made for the Cu-Ni resistivity ($\rho_m = 2.3 \times 10^{-7}$ Ωm) and the wire twist pitch ($L_p = 20$ mm), AC-losses can be calculated. The simulation results are comparable with experimental values as presented in Table III.

C. Conclusions

Calculations for the static magnetic refrigerators were validated and improved in terms of understanding the governing phenomena. With depicted numerical model further calculations for the FCC_ee prototype can be accomplished.

VI. FCC_EE PROTOTYPE DESIGN

Before performing detailed design of the static magnetic refrigerator for the FCC_ee, small scale prototype is designed and will be constructed. Additional improvements aimed at enlarging the cycle efficiency and cooling capacity will be introduced. The prototype characteristics are presented in Table IV.

Warm source cooling capacity is fixed to 1.1 W at 4.5 K in order to connect the prototype to existing cryogenic coolers in the laboratory. A magnetic field of 4 T can be achieved with standard superconducting coil. The chosen frequency of 0.1 Hz is a realistic assumption and gives room for optimization.

A. Thermal design

The paramagnetic material sizing has been performed with special care. Its length needs to be small enough to extract whole cooling capacity produced in the material. Maximal diffusion length L is a function of thermal diffusivity D and time τ allocated for the transformation:

TABLE IV. Small scale prototype parameters.

Cold temperature [K]	1.6
Warm temperature [K]	4.5
Power at the warm source [W]	1.1
Magnetic field [T]	0–4
Frequency [Hz]	0.1

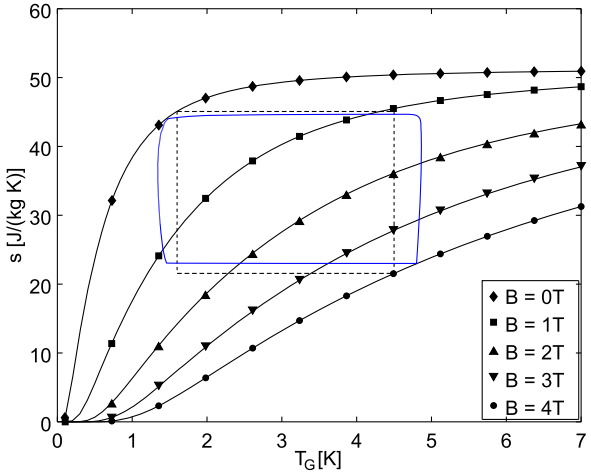

FIG. 7. Carnot cycle (dashed) and thermodynamic cycle taking into account heat exchange conditions on warm and cold sides (blue) of the designed prototype, without heat losses.

$$L = \sqrt{D\tau} = \sqrt{\frac{K}{\rho c_p}\tau}. \tag{5}$$

The mass of paramagnetic material depends directly on the frequency, magnetic field and targeted cooling power. For $f = 0.1$ Hz, a mass of 400 g of GGG should provide adequate cooling. GGG dimensions are calculated to 50 mm in length and 37 mm in diameter. Maximal length constraint is easy to satisfy in the small scale prototype. However, it is a stronger one for large power refrigeration and material research with design optimization should be performed to obtain larger conductivity and diffusivity values in the paramagnetic material.

Comparing the prototype calculation results (Fig. 7) with the Hitachi refrigerator (Fig. 5), one can notice smaller temperature differences between GGG and the heat sources in the cycle operating at lower frequency.

The lower the operating frequency the larger the time allocated for isothermal transformations. The cost is visible in lower volumetric cooling capacity ($\dot{Q}/V_G$) what increases the material amount and coil dimensions. In the designed prototype 4 T coil is used instead of 3 T one, what decreases magneto-caloric material size but increases the coil requirements.

Table V presents simulation results for two technical possibilities: with and without thermal switch at the

TABLE V. Small scale prototype calculations results.

Heat switch efficiency	100%[a]	0%[b]
Cooling capacity [W]	0.28	0.10
Power at the warm source [W]	1.1	1.1
Volumetric cooling capacity [W/dm^3]	5.0	1.7
Cycle efficiency η_c [W/W]	0.36	0.10

[a]Perfect heat switch.
[b]No heat switch.

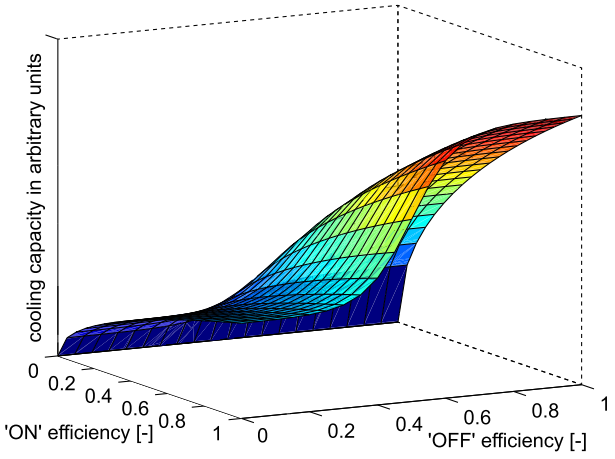

FIG. 8. Objectives for the heat switch efficiency.

GGG/warm source interface. Thermal switch provides perfect insulation in its OFF position (100% "OFF" efficiency) when GGG temperature is lower than the warm source temperature and does not modify the heat transfer during isothermal magnetization (100% "ON" efficiency). The goal of the heat switch design is therefore to minimize the heat transfer when GGG is cold and keep the exchange as efficient as possible when it is warm. In order to obtain cycle efficiency ($\eta_c > 30\%$), the heat switch efficiencies should be kept larger than 50% in both ON and OFF positions. Figure 8 presents the expected prototype performances accordingly to the ON and OFF heat switch efficiencies.

B. Heat switch discussion

Various possibilities of the heat switch design were investigated with the additional goal of keeping the simplicity of the construction. Various technical solutions which allow activating and deactivating the insulation cyclically are described below.

1. Solid layer heat switch

One can find materials with large variation of thermal conductivity in temperature so they could work as an insulation layer when GGG is cold and as a conductor when it is warm. An example of such material is sapphire which thermal conductivity varies 15 times between 1.5 K and 4.5 K [23]. In order to keep the temperature on the sapphire–warm bath interface higher than T_λ when $T_G < 1.5$ K, more than 24 cm of sapphire layer is needed (GGG thickness is 3.7 cm). In order to construct solid layer heat switch, a material with larger thermal conductivity change is needed but was not identified.

2. Gas heat switch

Heat switch adapted from the spatial adiabatic demagnetization refrigerators is a gas gap heat switch [24]. Thermal conduction is controlled by regulating the pressure in a gas cell. Very low pressure (10^{-5}–10^{-7} Pa) assures insulation and larger pressure (10^4–10^5 Pa) provides heat exchange. The heat flux in the OFF position is small enough even with 0.1–1 Pa and is independent on the gap. In the ON position, ΔT depends strongly on the gas gap thickness. The smallest technically achievable gap might reach 50 μm and for such thickness flux to the warm source reaches 950 $\mathrm{W/m^2}$. As a result, temperature at the heat switch-GGG interface would rise to 8.2 K what is not acceptable in the design. Furthermore, the gas heat switch cannot be successfully adapted due to very short time of the adiabatic transformation (seconds) in comparison to similar transformations in spatial systems (several minutes up to hours).

3. Mechanical heat switch

Various mechanical heat switches were studied: piston, iris mechanism, double trapdoor and windowed rotating mechanism. Chosen solution has to be reliable and leak-tight (the amount of liquid helium in the space between the heat switch and GGG should be fully removed or at least minimized). On the one hand, mechanical heat switch lowers the reliability of the whole refrigerator by introducing moving parts. On the other hand, it is the most straightforward solution which can satisfy both ON and OFF efficiency requirements and as a result significantly rise the cooling capacity of the system. A solution based on a windowed rotating mechanism that fulfills all the given requirements is under investigation in CEA-Grenoble.

VII. CONCLUSIONS

A mathematical model for static magnetic refrigerators was developed and gives a better understanding of the governing phenomena. This modeling work was used to design a small scale prototype to study possible improvements of the static magnetic refrigerators in the framework of the FCC design study. The development of an efficient mechanical heat switch is under investigation and is the key issue to validate the estimated performance improvements.

ACKNOWLEDGMENTS

This research was supported by CEA DRF Energy Program—DESA41K and CERN FCC Collaboration. We thank all colleagues from SBT and collaborating institutes, and acknowledge support from Christian Jeandey, Diego Paixao Brasiliano, Frederic La Rizza.

[1] L. Tavian, LHC Project Report No. 412, 2000.
[2] L. Couture and R. Zitoun, *Statistical Thermodynamics and Properties of Matter* (Gordon and Breach Science Publishers, Amsterdam, 2000).

[3] P. A. Bromiley, *Development of an Adiabatic Demagnetization Refrigerator for Use in Space* (Mullard Space Science Laboratory, University Collage of London, London, 1999).

[4] C. Delpuech, R. Beranger, G. Bon Mardion, G. Claudet, and A. A. Lacaze, Double acting reciprocating magnetic refrigerator: First experiments, Cryogenics **21**, 579 (1981).

[5] A. F. Lacaze, R. Beranger, G. Bon Mardion, G. Claudet, and A. A. Lacaze, Efficiency improvements of a double acting reciprocating magnetic refrigerator, Cryogenics **23**, 427 (1983).

[6] Y. Hakuraku and H. Ogata, A rotary magnetic refrigerator for superfluid helium production, J. Appl. Phys. **60**, 3266 (1986).

[7] Y. Hakuraku and H. Ogata, A static magnetic refrigerator for superfluid helium with new heat switches and a superconducting pulse coil, Jpn. J. Appl. Phys. **24**, 1538 (1985).

[8] Y. Hakuraku and H. Ogata, Thermodynamic analysis of a magnetic refrigerator with static heat switches, Cryogenics **26**, 171 (1986).

[9] M. Schmidt, *Contribution to the Development of a Cryogenic Magnetic Refrigerator Operating between 1.8 K and 4.5 K* (Fakultat fur Maschinenwesen der Rheinish-Westfalischen Technischen Hochschule, Aachen, 1992).

[10] S. Jeong, J. L. Smith, Y. Iwasa, and T. Numazawa, A regenerative magnetic refrigerator operating between 4.2 K and 1.8 K, AIP Conf. Proc. **273**, 619 (1992).

[11] G. K. White and P. J. Meeson, *Experimental Techniques in Low-Temperature Physics*, 4th ed. (Monographs on the physics and chemistry of materials, Oxford, 2002).

[12] T. Numazawa, K. Kamiya, T. Okano, and K. Matsumoto, Magneto caloric effect in $(Dy_xGd_{1-x})_3Ga_5O_{12}$ for adiabatic demagnetization refrigeration, Physica B (Amsterdam) **329–333**, 1656 (2003).

[13] R. A. Fisher, G. E. Brodale, E. W. Hornung, and W. F. Giauque, Magnetothermodynamics of gadolinium gallium garnet. I. Heat capacity, entropy, magnetic moment from 0.5 to 4.2 K, with fields to 90 kG along the [100] axis, J. Chem. Phys. **59**, 4652 (1973).

[14] Y. Hakuraku, Thermal conductivity of the gadolinium gallium garnet, $Gd_3Ga_5O_{12}$, between 1.4 K and 20 K, Jpn. J. Appl. Phys. **22**, 1465 (1983).

[15] B. Daudin, R. Lagnier, and B. Salce, Thermodynamic properties of the gadolinium gallium garnet, $Gd_3Ga_5O_{12}$ between 0.05 and 25 K, J. Magn. Magn. Mater. **27**, 315 (1982).

[16] W. Dai, E. Gmelin, and R. Kremer, Magnetothermal properties of sintered $Gd_3Ga_5O_{12}$, J. Phys. D **21**, 628 (1988).

[17] V. Arp, B. McCarty, and J. Fox, HePak, NIST technical note 1334, Software, v3.4. Horizon Technologies.

[18] R. J. Donnelly and C. F. Barenghi, The observed properties of liquid helium at the saturated vapor pressure, J. Phys. Chem. Ref. Data **27**, 1217 (1998).

[19] E. G. Brentari, P. J. Giarratano, and R. V. Smith, National Bureau of Standards Technical Report No. 317, 1965.

[20] Y. Hakuraku, Kapitza conductance of the gadolinium gallium garnet, $Gd_3Ga_5O_{12}$, between 1.4 K and 2.1 K, Cryogenics **24**, 156 (1984).

[21] A. Lacaze, Internal CEA Report No. SBT/LCF/85-06, 1985.

[22] P. Tixador and Y. Brunet, *Supraconducteurs—structure et comportement des fils* (Techniques de l'ingénieur, Matériaux à propriétés électriques et optiques, Editions T.I., Paris, 2004), http://www.techniques-ingenieur.fr/base-documentaire/materiaux-th11/materiaux-a-proprietes-electriques-et-optiques-42375210/supraconducteurs-d2702/.

[23] R. Berman, E. L. Foster, and J. M. Ziman, Thermal conduction in artificial sapphire crystals at low temperatures. I. Nearly perfect crystals, Proc. R. Soc. A **231**, 130 (1955).

[24] L. Duband, *A thermal switch for use at liquid helium temperature in space borne cryogenic systems*, Cryocoolers 8 (Plenum Press, New York, 1995), p. 731.